FLUID-STRUCTURE SIMULATION OF MULTIGAIT, JELLYFISH-LIKE LOCOMOTOR

By

AJAY DUSANE

A thesis submitted to the

School of Graduate Studies

Rutgers, The State University of New Jersey

In partial fulfillment of the requirements

For the degree of

Master of Science

Graduate Program in Mechanical and Aerospace Engineering

Written under the direction of

Aaron Mazzeo

And approved by

_____

_____

_____

New Brunswick, New Jersey

January 2018

ABSTRACT OF THE THESIS

FLUID-STRUCTURE SIMULATION OF MULTIGAIT, JELLYFISH-LIKE LOCOMOTOR

by AJAY DUSANE

Thesis Director:

Aaron Mazzeo

The current literature suggests that moon jellyfish are the most efficient underwater swimmers for their size. The objective of this thesis is to understand the gait- and material-specific fluid-structure interactions associated with the propulsion of moon jellyfish by simulating the motion, the mechanics, and fluid dynamics of moon jellyfish. The thesis uses a linear elastic material to describe the behavior of the silicone bell of the jellyfish made of Mold Star 30 and Ecoflex 30. Deflection-based experiments determined Young's modulus associated with these materials to be 1 MPa and 72 kPa, respectively for the range of strains typical of the flapping bell. To account for damping beyond that of the viscosity of the surrounding fluid, models incorporated Rayleigh damping or Maxwell and Kelvin-Voigt linear viscoelasticity. Parameters for these models came from the observed vibratory responses of elastomeric beams. Experiments and simulations with a flapping fin in water showed similar vortex shedding patterns.

The axisymmetric, laminar jellyfish-like numerical model developed emulates contraction of muscles in a moon jellyfish. The numerical model demonstrates the starting and stopping vortices mentioned in the literature. Understanding the fluid-structure interactions associated with the jellyfish motion, effects of changing the dynamics of the motion have the potential to influence the design of high-efficiency underwater vehicles.

ACKNOWLEDGEMENTS

It is my great pleasure to express my deep sense of gratitude to my advisor Prof. Mazzeo. His mentorship and encouragement led to the completion of the project.

I would like to thank Angela Straccia, Chandan Kumar, Harishanker Gajendran, and Temesgen Kindo from the COMSOL technical support, for their constant, unwavering support with the development of the numerical model.

Also, I would like to express my gratitude to Lilian Wang, Hillel Hochsztein, and Saleh Tahir for their assistance with the experiments. I would also like to acknowledge, Jingjin Xie, Tongfen Liang, Xiyue Zou for their guidance and support in the experiments.

Lastly, I would like to thank my reviewers, Prof. Denda and Prof. Diez.

DEDICATION

This thesis is dedicated to my beloved parents, sister, and my friends living across the oceans.

TABLE OF CONTENTS

LIST OF FIGURES

LIST OF TABLES

1. Introduction

Many of the design challenges that we face share commonalities with the challenges the rest of living beings have adapted with the evolutionary trial-and-error method. Nature has inspired many solutions and has continued to do so. Product designers focus on the structure and behavior of living organisms, entrepreneurs look towards the symbiotic relationship between ecosystem and its inhabitants, while research biologists study the biological kingdom. Biomimicry has inspired many solutions like noise reduction of the Japanese bullet train inspired by the beak of the kingfisher, the structure of the termite mound inspiring internal climate control system of a building, structure of mosquito's mouth leading to painless needle penetration and many more. Scientists and engineers are using these techniques to make the world a better place. This thesis focuses on biomimetic propulsion inspired by the moon jellyfish (Aurelia aurita) to make efficient underwater vehicles.

1.1 Medusae locomotion

The medusae employ jet propulsion for their motion [1]. The muscles in the bell contract and push water out from under its bell to propel itself forwards [2]. This generalization comes from many studies done on the swimming patterns of the medusae. Different medusae have evolved with varying patterns of swimming for survival. There are two broad categories of medusae, prolate and oblate species, depending on their bell shape. The size of the velum relative to the bell diameter determines the shape of the bell [1][3]. The prolate species have a large velum relative to their diameter while the oblate species have a smaller one. When the oblate species contract their muscles, the bell pushes the water from around and under down. A large vortex, also called the starting

vortex, forms at the margin of the bell. When they relax, the water refills the underside of the bell, forming a large vortex with vorticity opposite to that of starting vortex, called the stopping vortex. The repetition of the contraction and relaxation of the bell results in a series of closely spaced vortices as the medusa swims forwards.

According to Gemmell, et al. [4], the moon jellyfish might be one of the most efficient swimmers. They exhibit a phenomenon called passive energy recapture (PER). The moon jellyfish, an oblate medusa, contracts leading to the formation of starting vortex at the margin of the bell. It thrusts the jellyfish forward accelerating it to a maximum velocity. The jellyfish begins its relaxation phase shedding its starting vortex. The bell expands decreasing the pressure under the bell. It leads to water refilling in the underside of the bell and backward motion of the jellyfish. The backward velocity is smaller in comparison with the forward velocity attained during contraction, so the net movement is forward. During relaxation, the starting vortex merges with the stopping vortex under the bell, giving a low-velocity boost to the jellyfish. This phenomenon is called PER.

The jellyfish have evolved for survival, which includes feeding and propulsion. It is highly possible that the moon jellyfish can have higher efficiency if only propulsion was the only factor in its evolution.

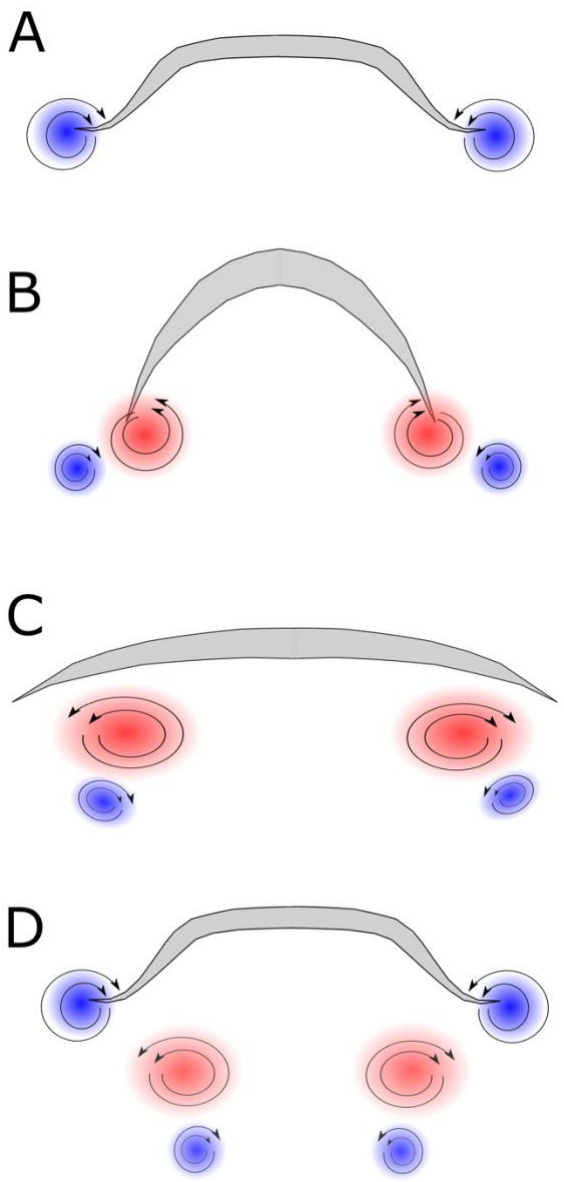

Figure 1. Schematic diagram depicting the vortices created during a swimming cycle of an oblate jellyfish. (a) During the contraction, the starting vortices form at the margin of the bell. (b) At the end of the contraction, the starting vortices shed off the bell and stopping vortices form under the margin of the bell. (c) During the relaxation phase, part of the starting vortices merges with and enhance the stopping vortices. The extra thrust demonstrates PER. (d) A new cycle begins with the formation of starting vortices. Copied from Lilian Wang's thesis.

1.2 Literature Review

Research into the locomotion of living jellyfish has occurred for decades. In the mid-1980s, T. L. Daniel described the hydrodynamics of jellyfish and concluded that the cost of locomotion was "nearly one order of magnitude greater than the extrapolated cost of locomotion for a vertebrate swimmer of equivalent body mass" [5], [6]. For many years, the belief was that "jet propulsion" with its rotating vortices during the contraction of the jellyfish was the sole mechanism behind the thrust and that the jellyfish, in general, were not very efficient as locomotors [7].

Just over ten years ago, Dabiri and Gharib started publishing works that further clarified the fluid mechanics behind marine propulsion of jellyfish and were able to derive and verify an expression relating the translational velocity of the jellyfish to the changing volume of the bell of the jellyfish and its area [8]. With Colin and Costello, they went on to further explore the flow patterns and the shedding of vortices with oblate medusa (jellyfish with the height of the bell less than their diameter), showing interactions between both starting vortices and stopping vortex [2], [9]–[13]. They overturned the belief that prolate jellyfish with jet propulsion were more efficient than oblate ones [1].

More recently, Gemmell et al. (including Dabiri, Colin, Costello, and Priya) concluded that oblate jellyfish are more efficient than many fish, making the jellyfish one of the most efficient underwater swimmers because of not only the timed interaction of stopping and starting vortices to cause a high burst in localized velocity and propulsion but "passive energy recapture" [4]. Passive energy recapture primarily results from the

stopping vortices running into the underside of the jellyfish to thrust it forward while it is coasting (i.e., there is no additional motion of the bell of the jellyfish).

The efforts to create jellyfish inspired locomotors are relatively recent compared to the decades of research spent on the locomotion of living jellyfish. The most mechanically developed prototypes have come from Priya's group at Virginia Tech and Tadesse at UT Dallas [14]. They have used shape memory alloys to contract the bell of the locomotor, "Robojelly." More recent works by the group point towards the fabrication of hydrogen-powered jellyfish locomotor. The heat generated by the reaction of hydrogen and oxygen with a catalyst actuate the shape memory alloys.

Another approach has been the tissue-engineered locomotor created by Nawroth Parker, Dabiri, and others [15]. By placing the muscle cells from rats, which contract under electrical fields, on pieces of silicone they were able to demonstrate jellyfish-like propulsion with starting and stopping vortices. However, its complexity of fabrication, low durability, and limited maneuverability act as a barrier to continued studies and motion.

The development of two way coupled numerical simulation is yet unseen. Gemmell et al. [4] used the geometry of living jellyfish (3 cm diameter) for the CFD analysis. They digitized the points along the contour of the jellyfish. They constructed a visually comparable curve representing the jellyfish bell, using interpolation, smoothening methods, and approximation. Coupling the motion of the jellyfish to the hydrodynamic forces exerted on the bell resulted in swimming motion. Pressure and shear forces integrated along the jellyfish boundary at the end of each time step, calculate the body acceleration. Using Taylor series expansion, they approximated acceleration

second order backward finite difference equation. They assumed laminar flow with axisymmetric geometry. The numerical simulations performed by Ramusssen, et al. [16] employ vortex particle method. They visualize the vortex dynamics associated with the self-propelled motion of jellyfish. However, the simulations performed were one way coupled to the medusa locomotion.

1.3 Objective

We explore the propulsion inspired by jellyfish locomotion. Several jellyfish-inspired robots developed by other research groups demonstrate the contraction and replicate the curvature of the bell of living jellyfish. Priya et al. [17] and Najem [18] built biomimetic jellyfish vehicles that use smart actuators, such as shape memory alloy (SMA) and ionic polymer metal composites (IPMCs), to bend the bell during contraction. These vehicles imitate the geometry of the bell for the deformation cycle. However, they do not focus on the analysis of the vortices formed during a contraction cycle or demonstrate passive energy recapture.

Our main objective is to design a vehicle that replicates the propulsion and swimming pattern of an oblate jellyfish. We want to visualize the flow field produced by jellyfish-inspired flapping motion, which could further extend to the understanding of vortex shedding of animals with fins, such as fish, jellyfish, eel, insects, and birds [19]. The numerical model will enable researchers to understand the dynamics of jellyfish-like propulsion. An in-depth study into the effects of the geometry, gait, material properties, and speed on the efficiency of the locomotor and vortex generation may result into an optimized underwater vehicle more efficient than the biological jellyfish. It reduces the effort of fabricating the jellyfish-based locomotor for every unique design.

This project develops a 2D two way coupled Fluid-Structure Interaction (FSI) simulation mimicking the jellyfish-like motion. The project uses a linear elastic material to simulate the low strains behavior of the silicone rubbers. We develop a 2D axisymmetric model which mimics jellyfish motion. We based the model on the fabricated jellyfish-like locomotor. We also analyze the fluid flow associated with flapping motion of fin using particle image velocimetry (PIV) for comparison.

1.4 Methodology

The project aims at making strides in developing a full-fledged three-dimensional dynamic simulation model representing jellyfish inspired locomotors. The project has three broadly defined phases.

In the first phase, we determine Young's modulus and dynamic parameters for the linear elastic material. In the second phase, we perform an FSI simulation with a rectangular fin made of Mold Star 30. We fixed the fin at one end and partially submerged it in water. The servo motor imparts oscillatory motion to the strip. The free end of the fin sheds vortices. This motion matches in the simulation model.

The approach for extracting hydrodynamic forces from velocity and velocity gradients would involve calculating the pressure. The pressure is often calculated by applying the Bernoulli equation outside the object wake to obtain the pressure on the boundaries of the selected control volume, and then applying a numerical integration scheme to resolve the pressure on the wake [20]. However, this method does not provide the pressure field, and the obtained boundary pressure depends on the direction of integration, increasing error. Another method for calculating pressure is using the pressure Poisson equation (PPE). However, a method proposed by Baur and Kongeter

[21] obtains instantaneous pressures from two dimensional, time-resolved particle image velocimetry (TR-PIV) measurements. It spatially integrates the pressure in four directions and takes the averaged values. The researcher will use the PIV method to obtain velocity, pressure, and velocity fields. Matlab offers a PIV toolbox developed by Dr. William Thielicke and Prof. Dr. Eize J. Stamhuis [22]–[24]. A video of the motion with tracker particles in the fluid is taken into consideration. The video is spliced into individual frames and fed into the toolbox. The toolbox analyzes a pair of consecutive frames for change in the position of tracer particles. By analyzing their motion, the toolbox can ascertain much useful information. We compare the vortices visualized by PIV to the simulation model for validation.

In the third phase, we construct a geometrical curve comparable to the actual fin of jellyfish inspired locomotor. We develop a COMSOL Multiphysics model mimicking the jellyfish-like locomotor motion.

1.5 Jellyfish-based soft locomotor

The research team at Rutgers fabricated a jellyfish-based soft locomotor. Ke Yang designed and fabricated the jellyfish [25]. Lilian Wang replicated the structure with modifications. The locomotor has soft bell structure from Mold Star 30 and Ecoflex 30. Mold Star 30 is the stiffer material chosen for the central region of the bell. It prevents the string from tearing into the bell. Softer Ecoflex 30 constitutes the rest of the bell structure. It allows the region near bell margin to deform with ease. We use soft lithography with 3D printed molds to make all the components of the bell structure.

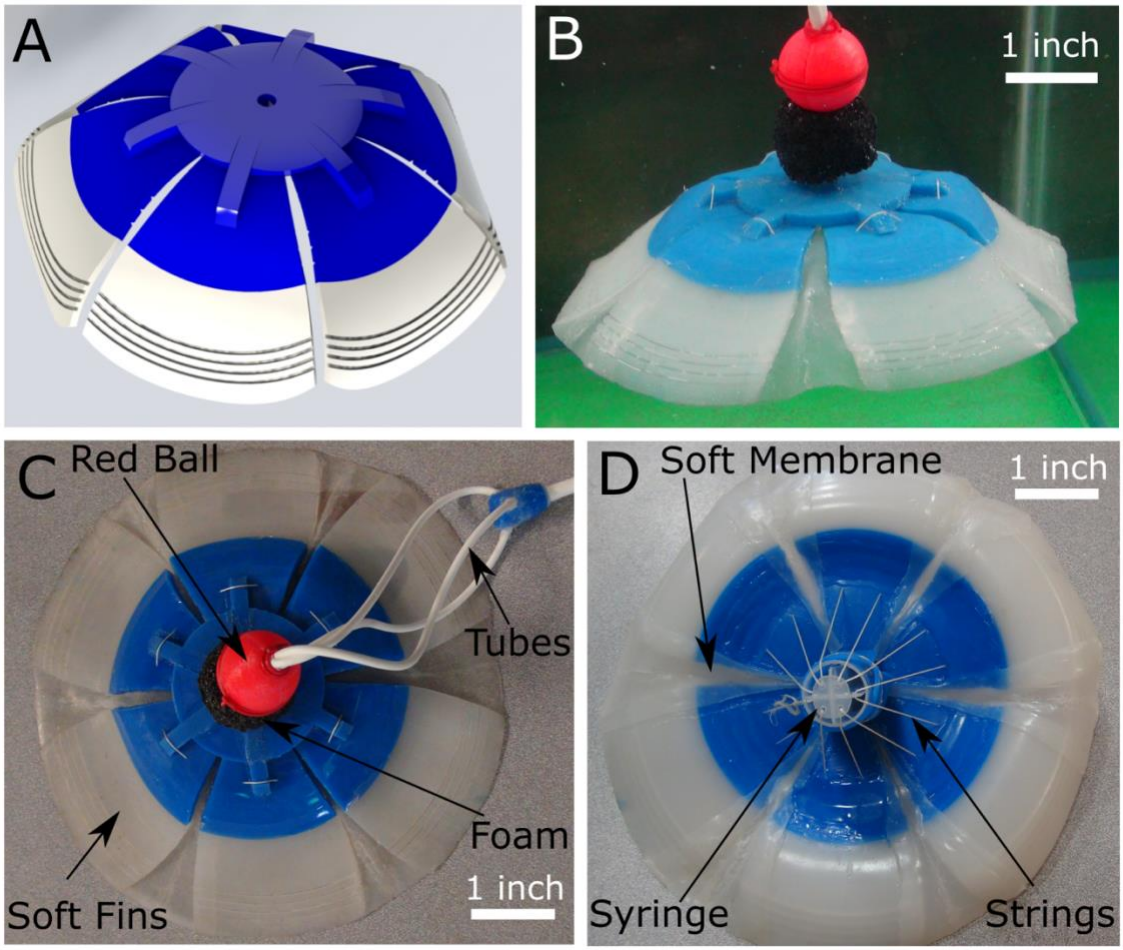

Figure 2. (a) Computer drawn isometric view of the locomotor with ideal curvature for the fin-like segments. (b) Perspective view of the locomotor in the tank to demonstrate the curvature of the bell in water. (c) The top view of the locomotor with six fin-like segments, a foam piece that points the locomotor upwards, a red ball used for tracking, and tubes to tether the locomotor to the control system. (d) The bottom view of the locomotor showing the soft connecting membranes, the string, and part of a 30-mL syringe. The string connected the end of the syringe to the underside of the bell structure. Copied from Lilian Wang's thesis.

2. Characterization of Material Model

The objective of the design of the soft locomotor is to replicate the shape of the bell and to mimic the movement of living oblate jellyfish. Other established soft robots inspired the design of the locomotor. The locomotor consists of a soft bell structure, a syringe, nylon string, and tubing. The design of the bell structure replicated the jellyfish-based robot presented in Ke Yang's thesis [25] with minor changes. The bell structure consists of six fin-like sections, small parts that connect the top of the fins, and thin membranes that connect the sides of the fins. The syringe expands in one direction linearly, and the string ties the end of the syringe to the underside of the bell of the locomotor. The linear actuation corresponds to the contraction and relaxation of the bell. The tubing delivers the water to the locomotor.

2.1. Fabrication

Fabrication of Rectangular strips/fin

We fabricated the rectangular strips from two types of silicone rubber, Mold Star 30 and Ecoflex 30. Mold Star 30 is a stiffer blue silicone rubber that is tear resistant, while Ecoflex 30 is a softer white translucent silicone rubber. We laser cut the acrylic sheet to make the mold for Mold Star 30 fin. We glued an uncut acrylic sheet to the base of the cut sheet. The mixture of Mold Star 30 was poured in this assembly and capped off by another acrylic sheet. It ensured high surface finish on all sides of the rectangular strip. 3D printing made Ecoflex 30 mold. For both Mold Star 30 and Ecoflex 30 rubbers, the liquid rubber consists of equally weighted two parts and requires degassing before mixing.

2.2 Linear Elastic Model

The soft bell structure of the Jellyfish-like locomotor is made up of silicone rubbers. These materials exhibit hyperelastic behavior. From the stress-strain curves for the hyperelastic materials, we can approximate a linear behavior for strain less than 10%. During the initial analysis, we observed that the strain generated in the bell structure is less than 10% except near the fixed constraint boundary condition. The area of interest is near the bell margin which has low strain values. Hence, assuming the linear elastic material model for these materials is justified.

In COMSOL Multiphysics, we simulate the linear elastic material model by considering material model as 'Nearly Incompressible Material.' This formulation is applied when the material under consideration has high Poisson's ratio. It avoids the phenomenon called *'locking.'* Due to near incompressible nature, the standard formulation results in undesirable effects; overly stiff models, checkerboard stress patterns, and errors or warnings from the solver due to ill-conditioning. The remedy is to apply *mixed formulation*, wherein, the pressure is an extra degree of freedom. The *mixed formulations* are enabled in the model when we check the 'Nearly Incompressible Material' checkbox in COMSOL Multiphysics.

2.3. Estimation of Young's Modulus

We estimated the Young's Modulus of the silicone rubbers by subjecting them to deformation due to self-weight. We clamped the rectangular strips of Mold Star 30 and Ecoflex 30 from the left end. The strips deformed under gravity resulting in curved deflection, captured with a graph paper in the background. The graph paper gave the numerical value of tip displacement and also eased superimposing experimental and

corresponding simulated deflection. The initial guess for Young's modulus, for the rubbers, was calculated using 100% Modulus and Hooke's law. 100% modulus is the value of the tensile stress at 100% elongation. These values are provided by the manufacturer. In literature, the recommended value of Poisson's ratio for rubbers is 0.49.

In COMSOL Multiphysics, we developed a model which simulated the gravity force on the body. The 'Parameter Sweep' functionality varies Young's modulus value over a wide range around the initial guess. The simulated deflection was visually compared with the experimental while also considering the deflection of the free end tip. We selected the value that best fit the criteria as the Young's Modulus of the material. We repeated the experiment for both, Mold Star 30 and Ecoflex 30.

Young's Modulus of Mold Star 30

A rectangular strip of dimensions, 105 mm x 38 mm x 2.1 mm was laterally hung with 16.7mm of the left side clamped. The initial guess for Young's Modulus is 0.66 MPa. The value of Young's modulus was varied from 0.5 MPa to 1.1 MPa in COMSOL Multiphysics model. We visually compared the deformed solid for every value with the experimental image. The best fit obtained was for 1 MPa.

Young's Modulus of Ecoflex 30

An Ecoflex 30 strip of the dimensions, 69 mm x 39 mm x 1.8 mm was considered, with longer edge fixed on the left side. Using the same method used for Mold Star 30, Young's modulus for Ecoflex 30 was determined. The 100% modulus for Ecoflex 30 is 68.95 kPa.

Table 1. Basic mechanical properties of Mold Star 30 and Ecoflex 30

	Density (kg/m3)	**Young's modulus (kPa)**	**Poisson's ratio**
Mold Star 30	1120	1000	0.49
Ecoflex 30	1070	72	0.49

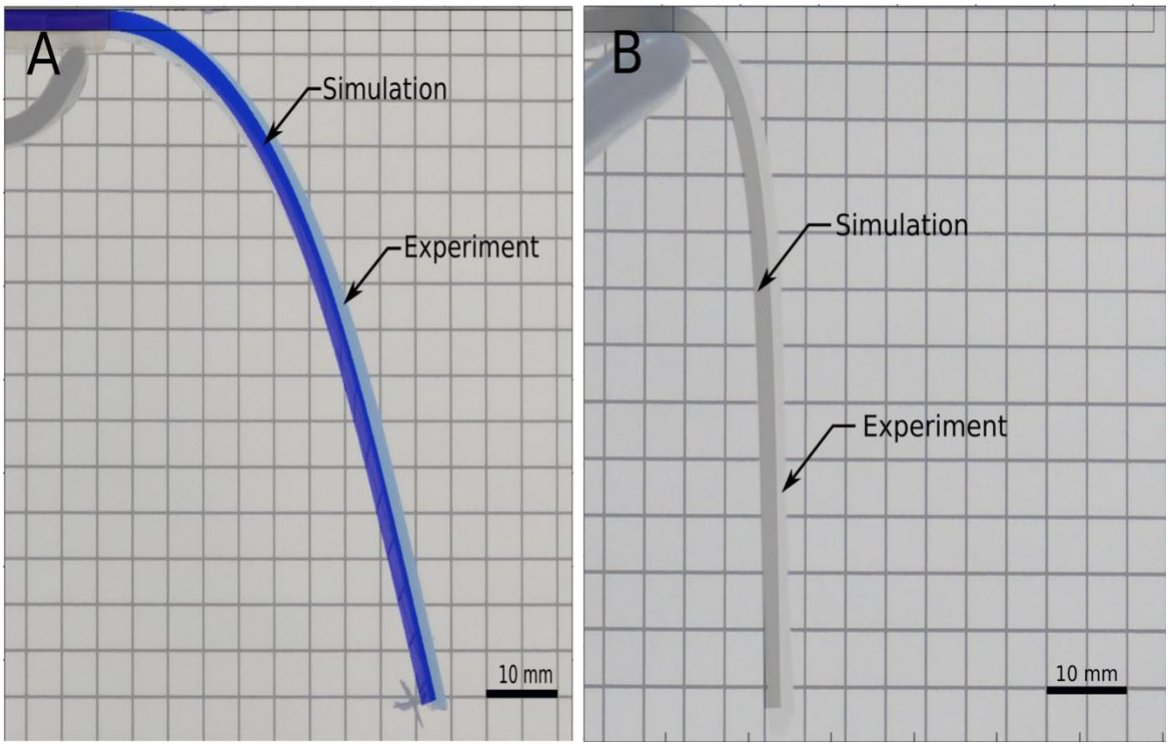

Figure 3. Comparison of experimental and simulated deformation for a) Mold Star 30 b) Ecoflex 30

2.4. Damping Characteristics

After determining the basic properties of the material, we performed initial validation experiment. We observed that the experimental and simulation behavior differed considerably. So to simulate the dynamic behavior more accurately, we investigated the effects of incorporating damping and viscoelastic characteristics. First, we investigate the effect of damping.

COMSOL Multiphysics offers three types of damping methods for a linear elastic material; Rayleigh Damping, Isotropic Loss Factor, and Anisotropic Loss Factor. We are considering the material to be isotropic. Hence we do not investigate anisotropic loss factor damping method. The motion of the jellyfish-like locomotor is time-dependent. Isotropic Loss factor method activates for frequency domain and not time domain. Hence, the only method available for damping is Rayleigh damping.

Rayleigh Damping

Rayleigh damping is a proportional damping method. It is proportional to the linear combination of mass and stiffness matrices. Due to its mathematically convenient formulation, it is widely used to model internal structural damping. The damping matrix is given by,

$$C = \alpha * M + \beta * K$$

where M and K are the mass and stiffness matrices respectively. α and β are the mass and stiffness damping parameters. One of the drawbacks of the Rayleigh damping is that it is frequency dependent. The stiffness damping parameter is linearly proportional to the frequency, while, mass damping parameter is inversely proportional to frequency. We experimented to determine the required damping parameters. The material strips were

hung vertically and were given an initial displacement at the bottommost region. The material strips freely oscillate in the environment like a pendulum. We neglect the effect of air resistance on damping. The camcorder captured the motion at 60 frames per second. The graph paper, in the background, with 1 mm graduations numerically characterized the oscillations. The central and extreme positions of the bottommost tip were noted for a number of successive oscillations and plotted in the MATLAB. The natural frequency and damping ratio of the materials were calculated using the following formulation,

$$\omega_n = \frac{2\pi}{T}$$

$$x(t) = \frac{x_0 \exp(-t\zeta\omega_n)}{\sqrt{1-\zeta^2}}$$

where, ω_n – natural frequency, T – time period, ζ – damping ratio, x_0 – Tip displacement at t = 0, $x(t)$ – time dependent response of the bottommost tip (exponential curve). Dividing the number of frames required to reach the extreme position in successive oscillations by the frames per second for the camera gives time period.

We performed two experiments on Mold Star 30 strip, with dimensions 105 mm x 2.1 mm x 38 mm, by varying its free length. In the first experiment, we clamped the strip at 10 mm of the length, which left 95 mm free for oscillation. In the second experiment, the free length is reduced to 85 mm.

We performed similar experiment with Ecoflex 30 strip of dimensions 69 mm x 1.8 mm x 19 mm with a free length of 63 mm.

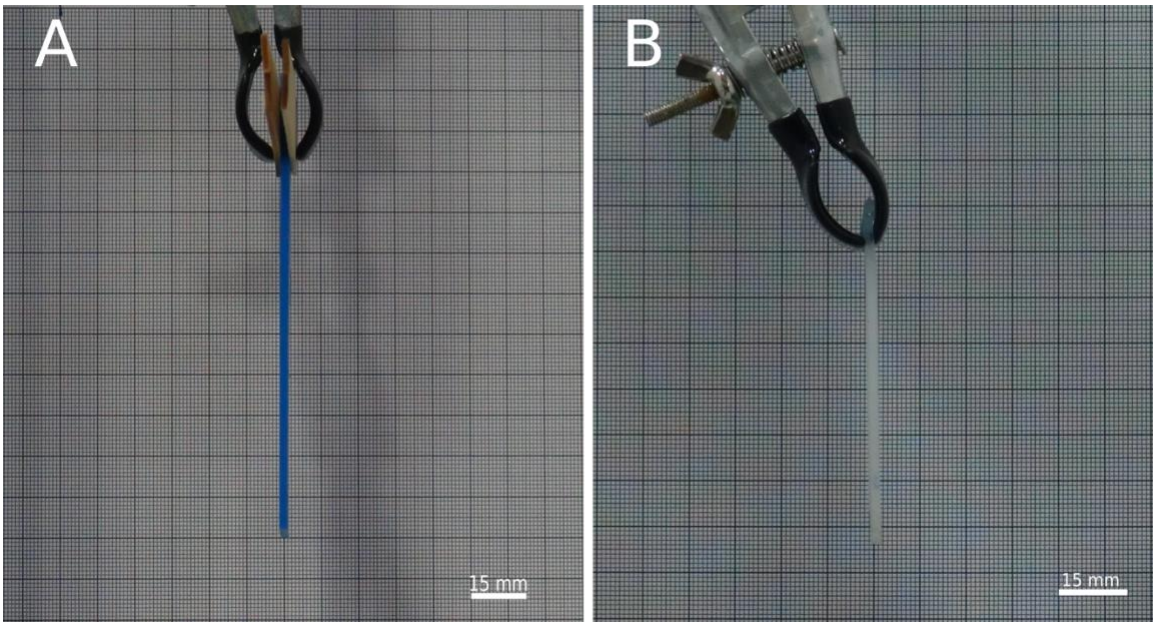

Figure 4. Experimental setup for a) Mold Star 30 b) Ecoflex 30. Displacement applied to the bottom portion of the strips.

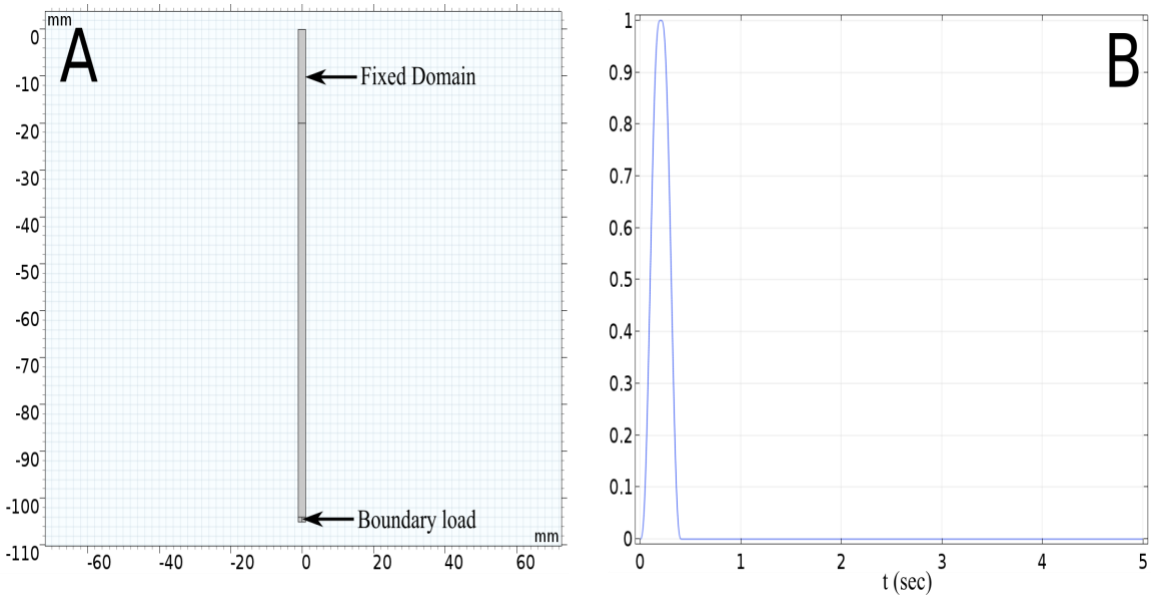

Figure 5. COMSOL Multiphysics model a) Position of boundary load. b) Time-dependent unit force.

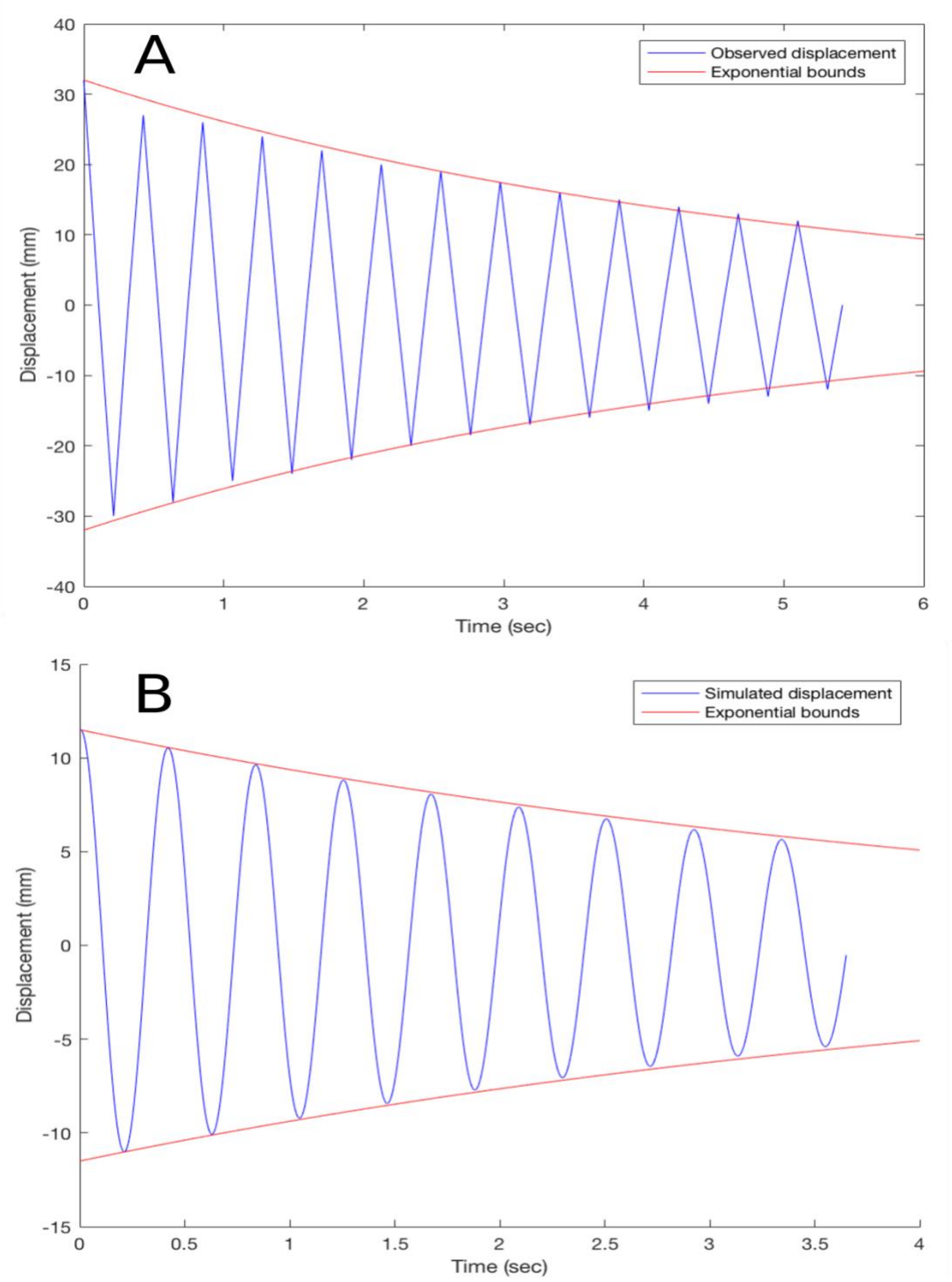

Figure 6. a) Observed tip displacement of Mold Star 30. b) Experimental tip displacement of Mold Star 30 with Rayleigh damping. The exponential bounds for experiment, represented in red, match with the simulation.

In COMSOL Multiphysics, we developed a model simulating the oscillatory motion. Gravity force acts on all the domains. Force acts on the bottommost part as a time-dependent rectangular function shown in **Figure 5**. After the initial displacement due to the applied force, COMSOL Multiphysics simulates the oscillatory motion using Time-Dependent study. The time-displacement data of the bottommost point is gathered from the results and exported to MATLAB for further analysis. After some trial and error, the damping ratio is found out. Depending upon the value, a new guess for Rayleigh parameters is considered and plugged in the numerical model. We repeated this process till the damping ratio for experiment and simulation match.

Table 2. Damping parameters for Mold Star 30 and Ecoflex 30

	Rayleigh parameters	
	$\boldsymbol{\alpha}$	$\boldsymbol{\beta}$
Mold Star 30 (Exp 1)	0.2	0.001
Mold Star 30 (Exp 2)	0.1	0.001
Ecoflex 30	0.015	0.0015

2.5. Viscoelastic Characteristics

Linear viscoelasticity is a reasonable approximation to the time-dependent behavior of polymers. We consider Generalized Maxwell Model and Kelvin-Voigt Model for the analysis. COMSOL Multiphysics requires additional properties while defining the viscoelastic material. Shear Modulus (G) and Relaxation Time (τ_v) are the two properties required by both, Generalized Maxwell and Kelvin-Voigt Models.

Shear Modulus is given by,

$$G = \frac{E}{2(1+\nu)}$$

Relaxation time (τ_v) is the material property which is varied to match the experimental damping ratio/natural frequency with the simulated one. It is the ratio of linear dashpot constant to the linear spring constant.

The Generalized Maxwell model consists of N different Maxwell units in parallel. A Maxwell unit is spring and dashpot in series. In Kelvin-Voigt model, spring and dashpot are connected in parallel.

Table 3. Viscoelastic parameters for Mold Star 30 and Ecoflex 30.

	Shear Modulus (kPa)	**Relaxation Time (sec)**	
		Generalized Maxwell	**Kelvin-Voigt**
Mold Star 30 (Exp 1)	335.57	0.0064	0.0064
Mold Star 30 (Exp 2)		0.004	0.004
Ecoflex 30	24.161	0.02	0.02

As seen in the table above, the values of the damping and viscoelastic parameters change with the geometry. We take these values as reference points for further analysis and not as absolute material properties.

3. Fluid-Structure Simulation

3.1 Fluid-Structure Interaction theory

Fluid-Structure Interaction is a multiphysics coupling between Fluid Dynamics and Structural Mechanics. FSI comes into play when there is movable or deformable solid body surrounded by a fluid. Fluid-Structure Interactions are crucial in the considerations of the design of engineering systems dealing with any fluid. The effect of fluid on the solid and the consequent effect on the fluid itself is the crux of FSI analysis. In our modeling and analysis, we make use of FSI module to determine the dependencies of vortex shedding process.

COMSOL Multiphysics has a preconfigured FSI module in its package, which combines the Fluid Mechanics and Structural Mechanics module. COMSOL Multiphysics uses Arbitrary Lagrangian – Eulerian (ALE) method to solve FSI problems. The Lagrangian algorithm is mainly used to solve Structural Mechanics problems. Use of material domain allows easy tracking of free surfaces and interfaces. However, it cannot handle large distortions of computational mesh. The Eulerian algorithm, on the other hand, is used to solve Fluid Mechanics problems. The spatial domain can handle large distortions but at the expense of interface tracking. ALE aims at combining the advantages of both the algorithms. It makes it possible to track surfaces and interfaces, simultaneously handling large distortions. ALE uses a referential configuration for the description of motion. FSI module of COMSOL Multiphysics inherently solves for geometric non-linearity.

Governing Differential Equations:

FSI module primarily solves for three equations, Navier Stokes, Continuity, and time-dependent displacement of solid.

$$\rho \frac{\partial u_{fluid}}{\partial t} + \rho(u_{fluid} \cdot \nabla) u_{fluid} = \nabla \cdot \left[-\rho I + \mu \left(\nabla u_{fluid} + (\nabla u_{fluid}) \right)^T \right] + F$$

$$\rho \nabla \cdot u_{fluid} = 0$$

$$\rho \frac{\partial^2 u_{solid}}{\partial t^2} - \nabla \cdot \sigma = F_v$$

where, u_{fluid} - is fluid velocity field,

ρ - fluid density,

I – Identity matrix,

u_{solid} – displacement field.

The above equations solve for dependent variables, fluid velocity field and pressure, solid displacement field, and auxiliary pressure for solid (when considering *mixed formulations*). COMSOL Multiphysics adds additional variables with the addition of Dirichlet or Neumann boundary conditions and material properties like damping and linear viscoelasticity.

3.2 Particle Image Velocimetry

PIV is a non-intrusive, quantitative and qualitative flow visualization technique. In this technique, reflective and neutrally buoyant tracer particles seed the fluid. These particles follow the fluid motion. The desired fluid dynamics are observed by illuminating the fluid and recorded. For successive times steps, the images are compared, and change in the position of the particles is noted. Velocities can be derived by noting the time difference between the frames and change in position of the particles.

PIVlab is a Time-Resolved Digital Particle Image Velocimetry tool programmed with MATLAB by Dr. William Thielicke and Dr. Eize J. Stamhius. Images of the motion under consideration are uploaded in the software. The tool has options for selecting the region of interest, masking, image preprocessing techniques, interrogation window size, and selecting the algorithm for analysis. Post-processing tools allow us to visualize fluid velocity, vorticity, and other parameters. We recorded the fluid motion at 60 fps. The video is spliced into individual frames and imported in the toolbox.

3.3. Simulating Rectangular Fin

A validation experiment was conducted to ascertain the ability of the approximated model to simulate the vortices. We consider a rectangular strip (105 mm x 2 mm x 95 mm) of Mold Star 30. The partially submerged rectangular strip oscillates angularly with one extreme fixed and the other one free. The servo motor controlled by Arduino Uno applies the oscillatory motion. This angular motion is transferred to the fin using wooden tongue depressors. The motion leads to shedding of vortices at the tip of the free end. We performed the experiment in a water tank. The camcorder captures the motion at 60fps. The glitter particles seed the fluid volume for PIV analysis.

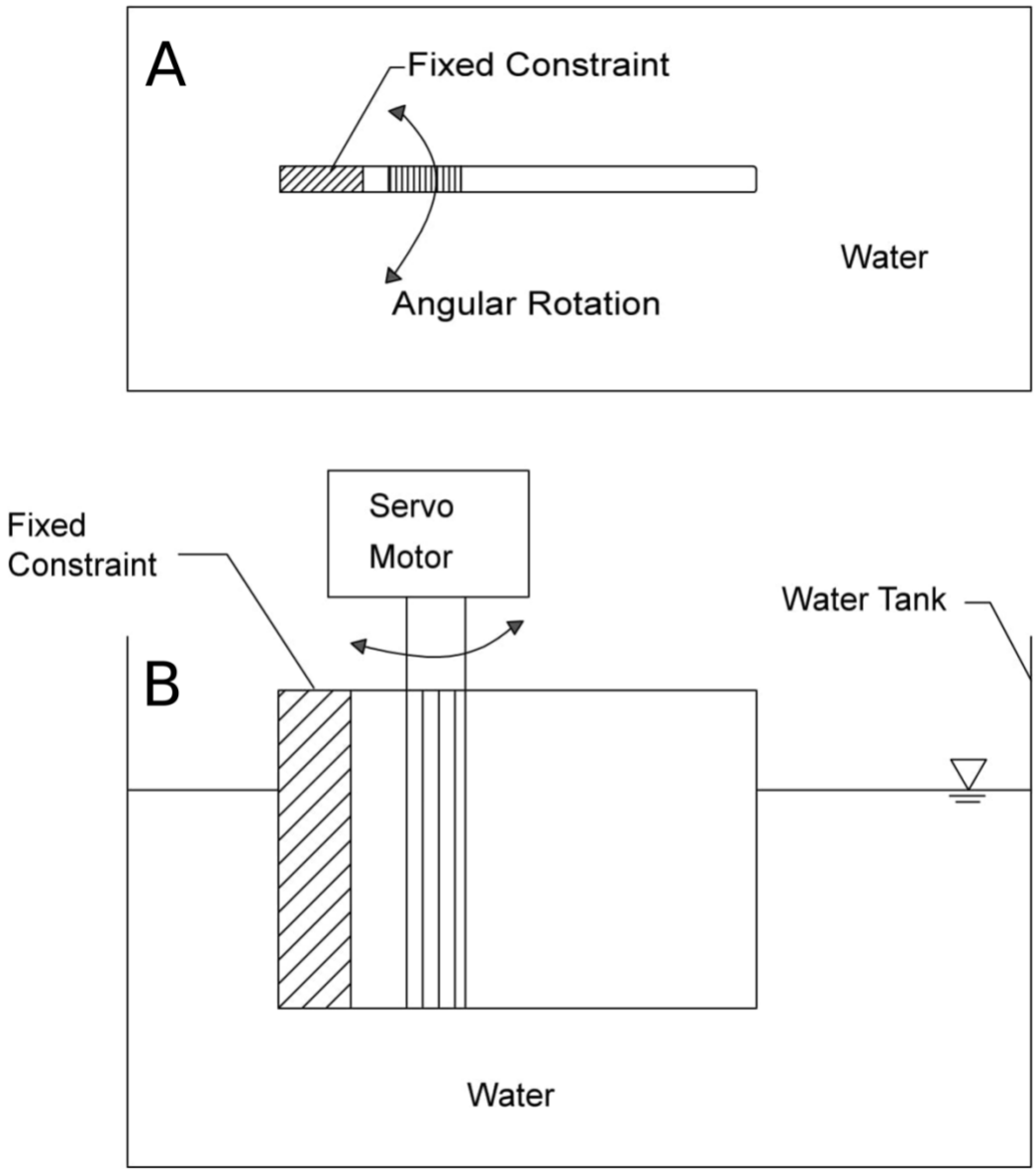

Figure 7. a) The schematic representation of the oscillatory angular motion of the rectangular fin. b) Schematic representation of experimental setup for the validation experiment.

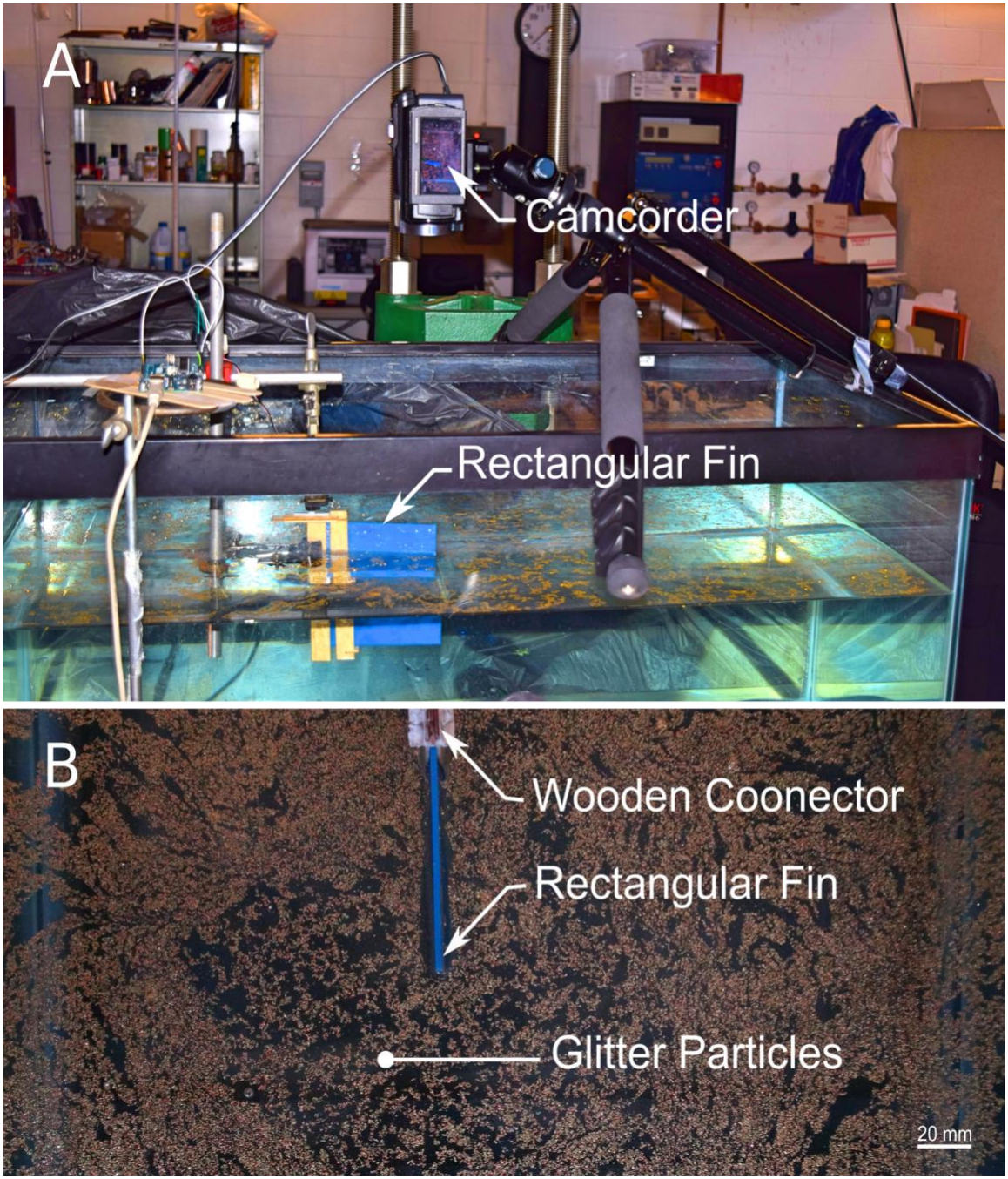

Figure 8. (a) The experimental setup with the rectangular fin partially submerged in the water tank. (b) Top view of the experiment. The wooden connector transfers the oscillatory angular motion to the rectangular fin. The glitter particles seed the fluid volume for PIV analysis.

COMSOL Multiphysics Model

We use the FSI module of the COMSOL Multiphysics. In FSI module, we provide the necessary boundary conditions for the fluid domain. The solid domain is modeled as linear elastic material with damping or viscoelasticity. The oscillatory angular motion is modeled using a special kinematic constraint called 'Rigid Connector.' In this feature, the selected geometric entities act like rigid bodies. Not only this feature simplifies the simulation but also allows to specify the rotation of the rigid bodies. The angular displacement due to the wooden connector is accurately modeled using this feature.

The two geometric lines are constructed within the material at equidistant from the top and bottom edges. These lines are selected in the 'Rigid Connector' feature. The rectangular fin oscillates at an amplitude of 10 degrees with sine function of time period 1.25 sec as the input signal in the experiment. The displacement at the center of rotation is zero. The coordinates for the center of rotation is the center of the servo motor, noted with reference to the rectangular fin. The underlying assumption that the material held in between the wooden connector is rigid is justified as the material is tightly held. No deformations take place in that region.

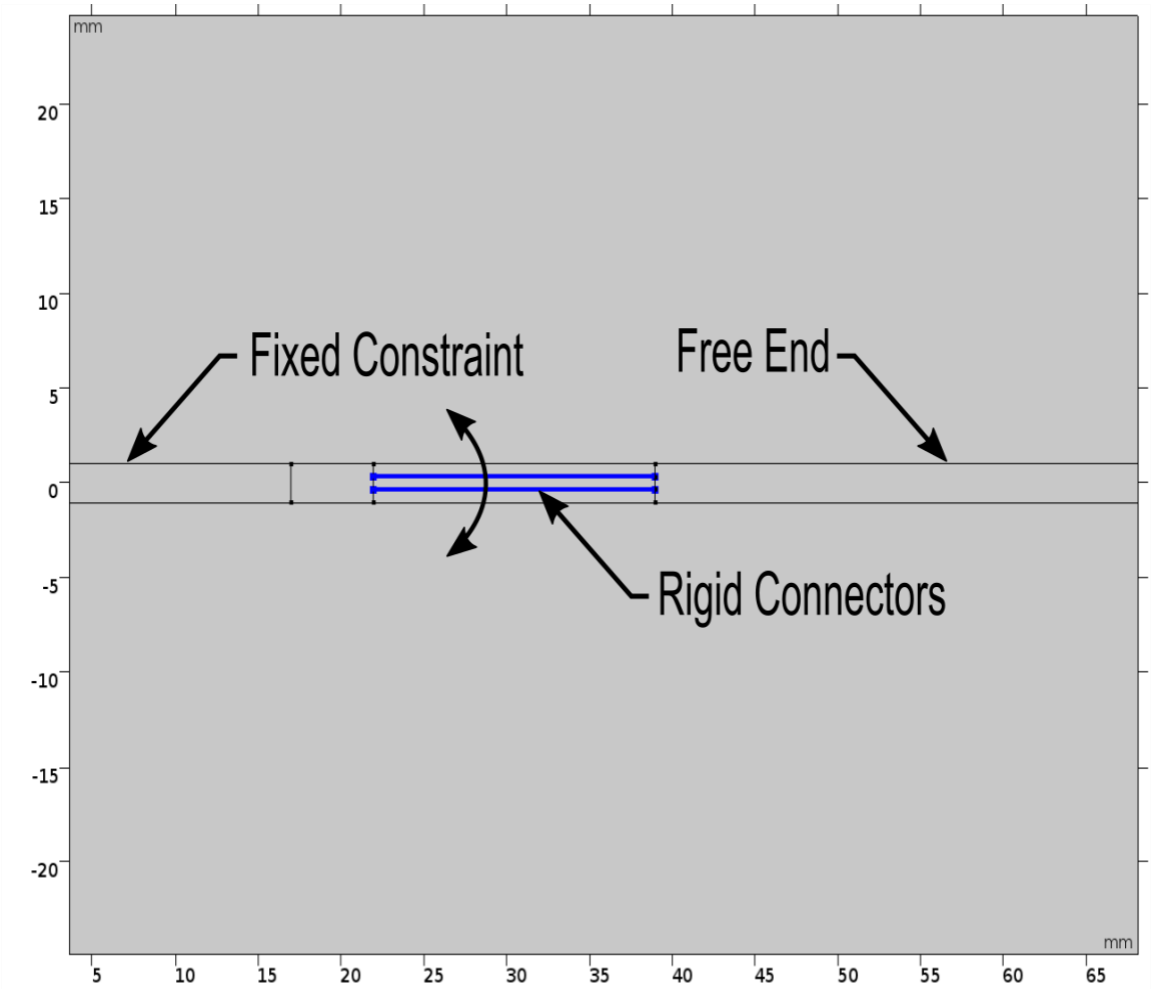

Figure 9. Cropped image of the COMSOL Multiphysics FSI model. The highlighted lines in blue are the Rigid Connector boundary conditions. These boundaries experience oscillatory angular rotation defined by a sine function.

3.4. Axisymmetric Jellyfish-like locomotor

Geometry

The geometry of the model is a 2D cross-section of the jellyfish-like locomotor fabricated by Ke Yang [25]. We determined the geometry by measuring the dimensions of the fabricated locomotor, drafted it in AutoCAD, and exported it to COMSOL Multiphysics. The geometry has no sharp edges and corners have appropriate fillet radius. The 'Solid Mechanics' module imported the AutoCAD geometry and performed the static analysis. We applied the gravity force on the initial geometry, which produced the curvature of the fin. We remeshed the curved geometry and exported it to the FSI module for a time-dependent study. We initially constructed a 2D geometry and then moved to 2D axisymmetric. We initially constructed a 2D geometry and then moved to 2D axisymmetric. The axes changed from x and y to r and z, respectively. However, equations of motion remained unchanged.

Flow Assumption

In the FSI analysis, we assume laminar flow for the numerical model. Laminar flow transitions into turbulent one at Re > 5 x 10^5. We calculate the Reynolds number as

$$Re = \frac{\rho V D}{\mu}$$

where, ρ – fluid density, V – fluid velocity, D – bell diameter, μ – dynamic viscosity of fluid. The Reynolds number for D – 0.21m, V – 0.3 m/s is 70786. Hence, the assumption of laminar flow is valid.

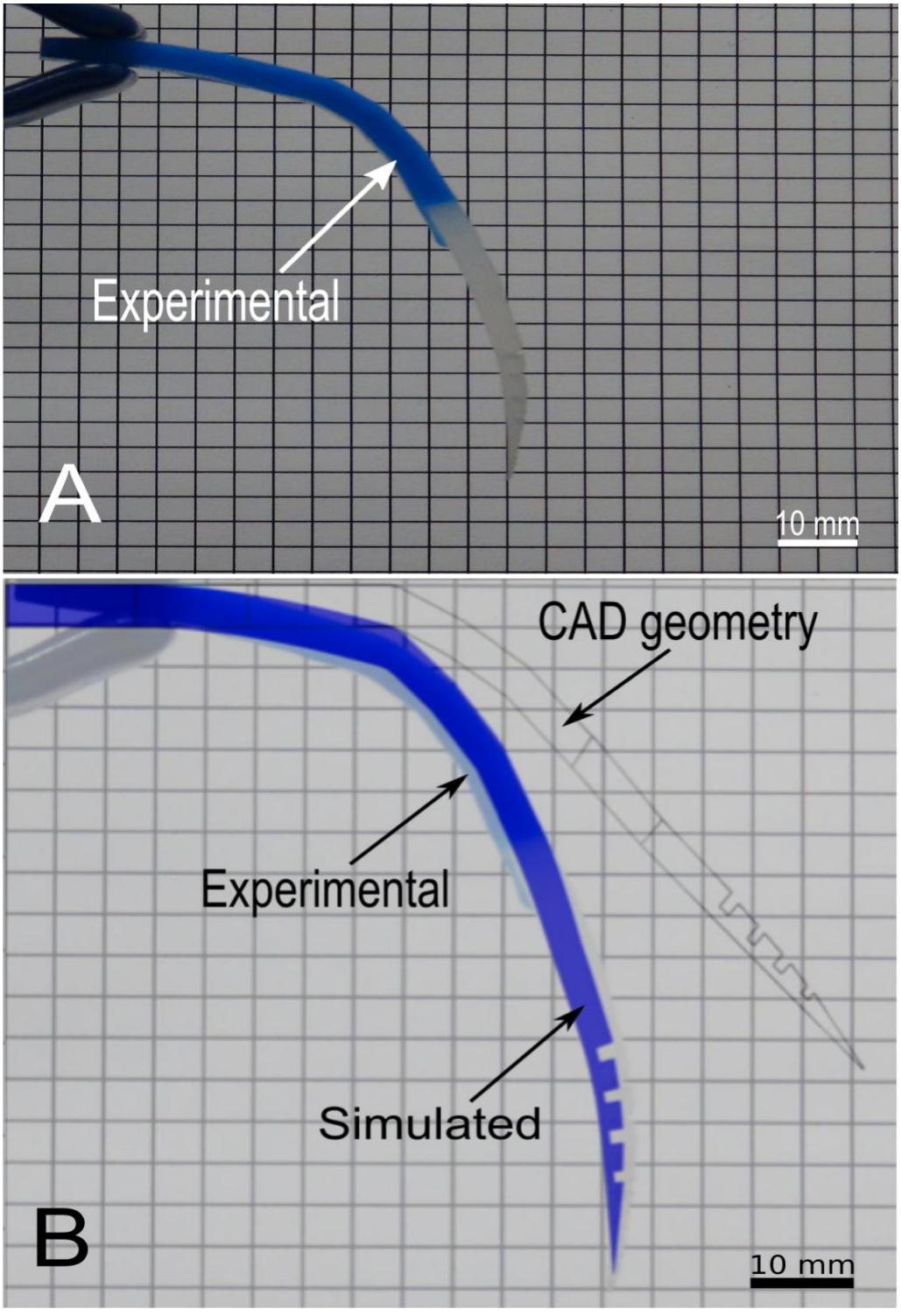

Figure 10. a) Jellyfish-like fin composite of Mold Star 30 and Ecoflex 30. b) Superimposed geometry of simulated and experimental fin. Simulated geometry is the result of the gravity force acting on the CAD geometry.

Prescribed Displacement

The jellyfish-like locomotor, tethered to a hydraulic system, is controlled by motorized linear actuators. The flapping motion has four stages, viz., contraction, coasting, relaxation, and post-relaxation period. Proportional-integral-derivative (PID) controller and pulse width modulation (PWM) controls the motion of the linear actuators. The linear actuators hydraulically actuate the piston-syringe arrangement on the locomotor. The string connects the syringe to the bell structure. The point at which string meets the bell structure is the point of interest. We determined the initial and final positions of this point. We approximated the intermediate displacement in the following manner. The time-dependent linear position (Ys) of the syringe is known, and length of the string (Ls) remains constant throughout the motion. We assumed that the angle of the string with the vertical changes linearly with respect to time. Using trigonometry, we split the sinusoidal displacement in 'r' and 'z' directions. In the numerical model, we prescribed this displacement to the same point. To avoid singularities, we applied the displacement over adjoining area, which in this case is a line. In a periodic motion, it is imperative that end of the previous cycle and the start of the new cycle occur at the same point. Any mismatch in the position will lead to numerical instabilities and non-convergence of the solution. To avoid this, we have used 'ramp' function for the contraction phase. The 'ramp' function slowly ramps up the prescribed displacement without affecting the desired displacement in a meaningful way.

In the coasting phase, the model maintains the same position as at the end of the contraction phase. The relaxation phase has a linear profile for both the directions. Linear functions start at the end of the coasting phase and end at the zero displacements. Post

relaxation period maintains this position for the specified time. The displacement functions are parameterized, allowing a change in the duration of each phase. The magnitude of the displacement can also vary. The model achieves its goal of being multi-gait capable.

Equations of motion

$$\theta(t) = \theta_i - \frac{\theta_i - \theta_f}{Tp} * t$$

$$Ys(t) = 63.55 + StrokeLength * \sin\left(\frac{2\pi t}{T}\right)$$

$$Xc(t) = \left(-35.4 + L_s * sin\big(\theta(t)\big)\right) * ramp(t)$$

$$Yc(t) = \left(L_s * cos\big(\theta(t)\big) - Ys(t)\ \right) * ramp(t)$$

$$Xr(t) = \left(\frac{0 - Xc(t)}{rst}\right) * (t - stc - coast - rst)$$

$$Yr(t) = \left(\frac{0 - Yc(t)}{rst}\right) * (t - stc - coast - rst)$$

$$X(t) = \begin{cases} Xc(t), & t < stc \\ Xc(stc), & stc < t < coast \\ Xr(t), & coast < t < rst \\ 0, & rst < t < prp \end{cases}$$

$$Y(t) = \begin{cases} Yc(t), & t < stc \\ Yc(stc), & stc < t < coast \\ Yr(t), & coast < t < rst \\ 0, & rst < t < prp \end{cases}$$

where,

StrokeLength – dead length of piston,

T – time period of the displacement cycle, Tp = T/4,

Ls – length of string,

Xc(t) – contraction function in r or x direction,

Yc(t) – contraction function in z or y direction,

Xr(t) – relaxation function in r or x direction,

Yr(t) – relaxation function in z or y direction,

X(t) – piecewise function in r or x direction,

Y(t) – piecewise function in z or y direction,

stc – contraction time, coast – coasting time,

rst – relaxation time, prp – post relaxation time.

Using COMSOL Multiphysics smoothes the individual displacement functions to get a continuous displacement function. Ramp function smoothly applies the contraction displacement to a avoid sudden jump in the displacement.

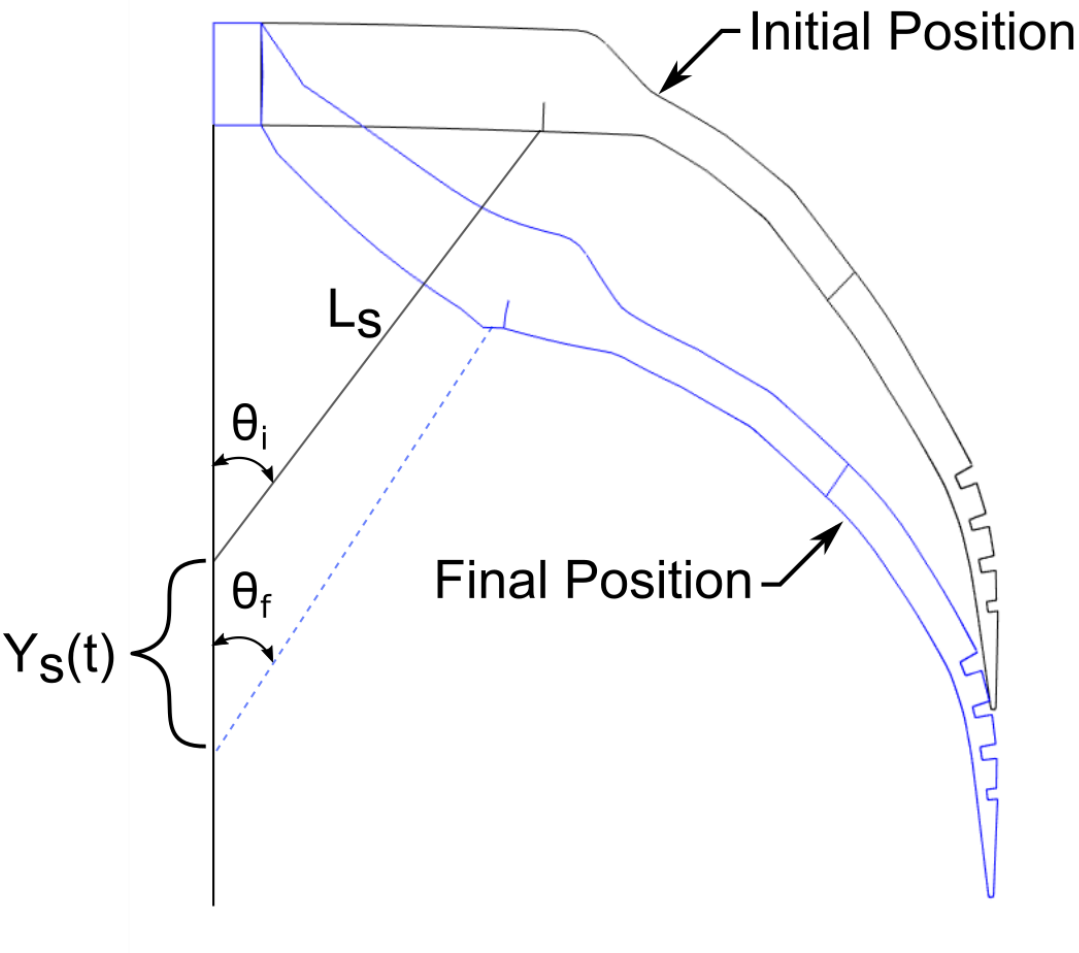

Figure 11. Initial and final position of the jellyfish-based locomotor, highlighted in black and blue color, respectively. The syringe undergoes oscillatory linear motion. Ys(t) is the time-dependent position of the syringe. Ls is the length of string from the syringe to the bell structure.

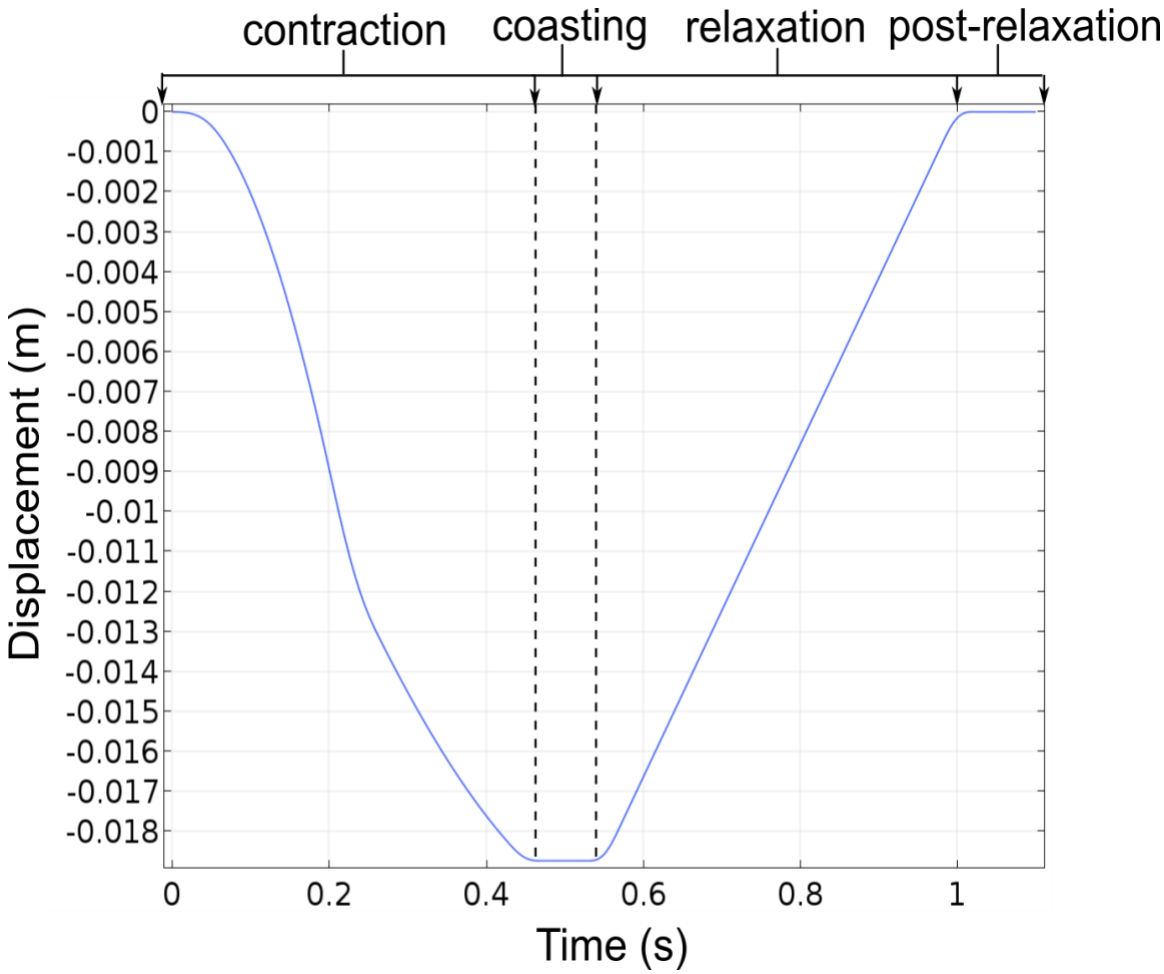

Figure 12. Different stages of the fin displacement in the z-direction. The displacement has four stages, contraction, coasting, relaxation, and post relaxation. Displacement in r-direction has a similar curve. The duration, rate of change, and amount of change for each stage is customizable.

Meshing

The model has different size settings for the fluid domain and the solid domain. Mesh for the solid domain is finer than for fluid domain. ‘Corner Refinement’ feature in COMSOL Multiphysics refines the mesh at small corners. It ensures optimal mesh element growth near critical areas of the solid and fluid domains. The locomotor undergoes a considerable amount of displacement. During the initial analysis, we observed, failing of mesh near critical areas. Due to large displacement, the mesh elements invert leading to divergence of the solution. It is a major source of concern. We employed the ‘helper lines’ to help the mesh with the displacement, usually when the displacement of a point is unknown. ‘Helper lines’ move the mesh according to the displacement of the specified point. It prevents inversion of the mesh elements. However, ‘helper lines’ should be employed only on specific points. ‘Helper lines’ when applied inappropriately can lead to mesh element inversion.

4. Verification of Simulation and Results

The rectangular fin experiment is a validation experiment for FSI module. We judge the validation in two ways. Firstly, we compare the tip displacement data for experiment and simulation. The rightmost tip of the fin sheds the vortices. We spliced the video into individual frames and tracked the displacement of the tip for each frame. We plotted this data with respect to time. In COMSOL Multiphysics, using 'Point Evaluation,' we exported the simulated tip displacement data. This information is imported in MATLAB and compared with the experimental plot. The parameters used are the ones mentioned in Table. The numerical model sheds vortices in phase with the experiment. From the **Figure 13**, we can observe that crests and troughs are in almost in-phase. Rayleigh and Viscoelastic methods discussed earlier are dependent on structure. Any change in structure will lead to change in the respective parameters. **Figure 13** shows the comparison of tip displacement of rectangular fin for the experiment (red) and simulation (simulation). The vortices shed about the same, except the amplitude of the tip displacement is dissimilar. The experiment used a rectangular fin with larger dimensions than the one used for the calculations in **Table 2**. The result is congruent with the previous analysis. Fig. shows the overlay of experiment and simulation of rectangular fin.

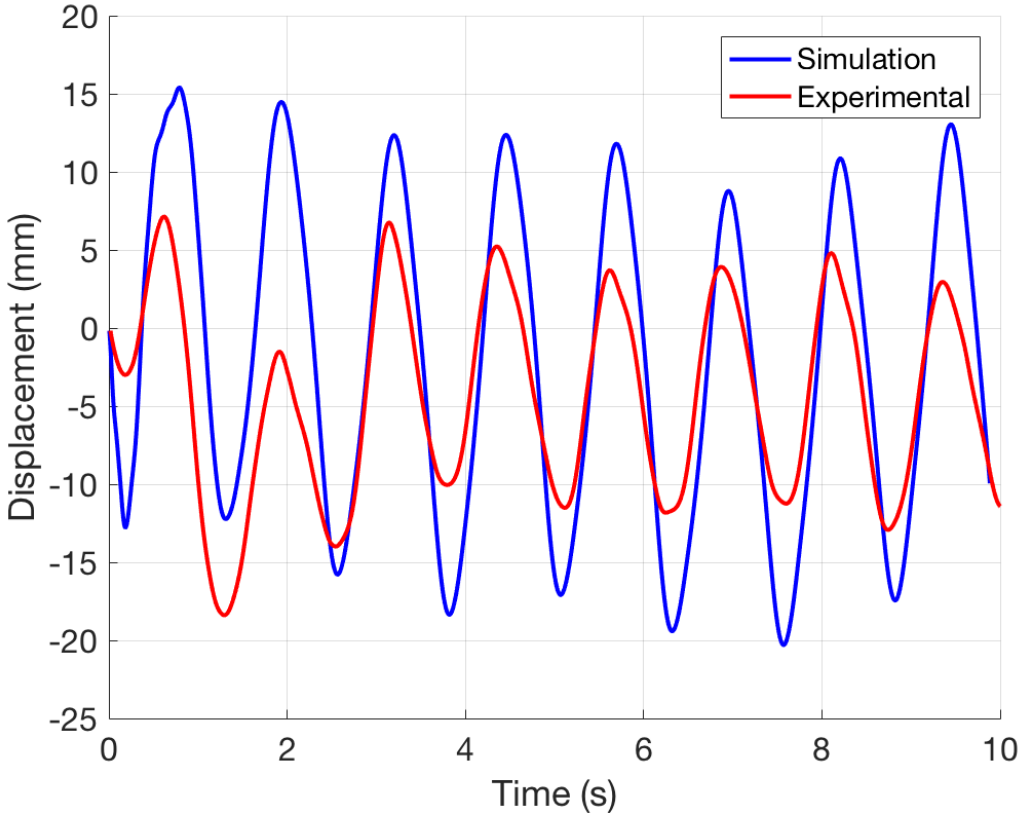

Figure 13. Comparison of simulation and experimental tip displacement for Rayleigh damping. The extremes of the curves are almost in-phase.

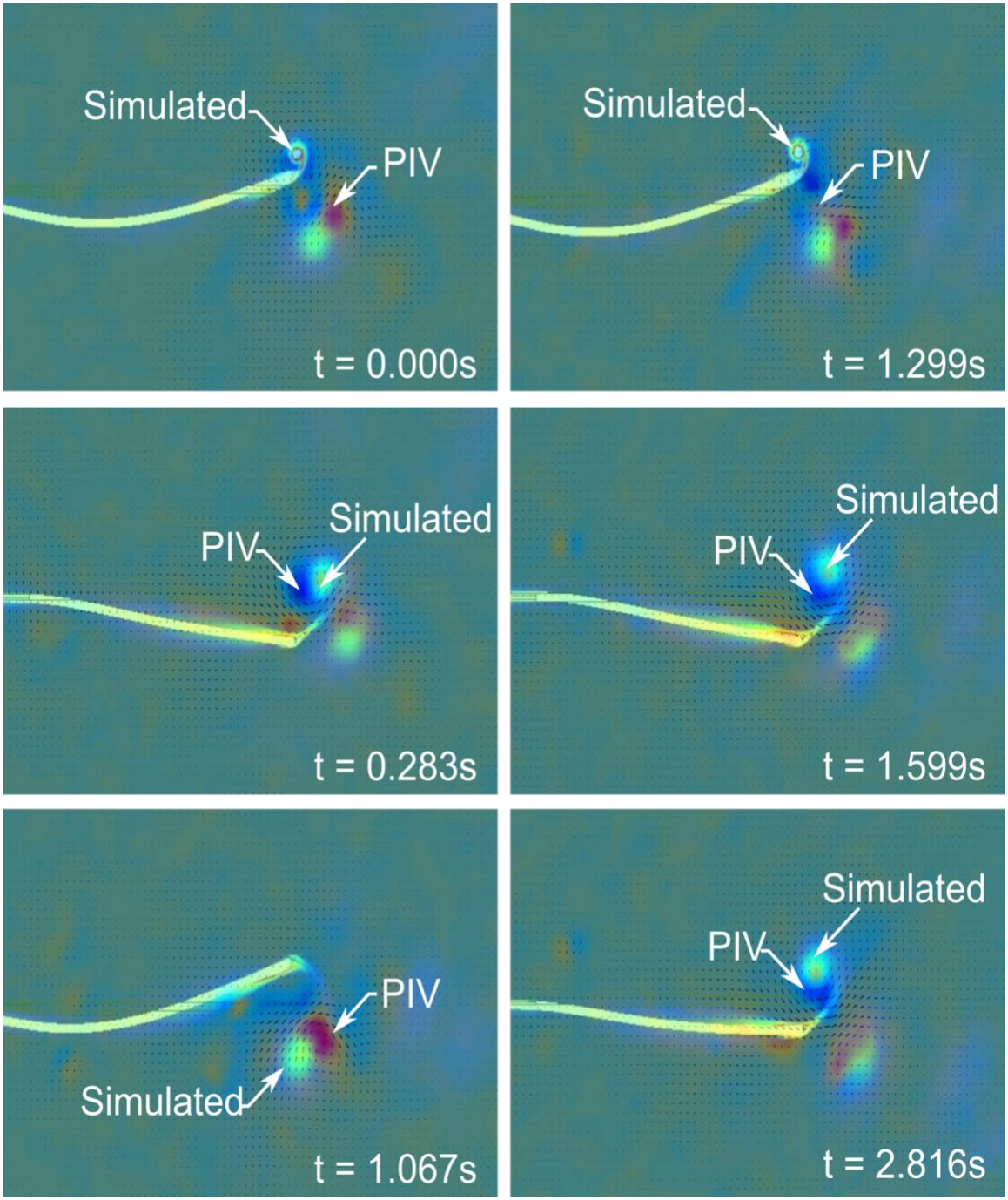

Figure 14. Experimental and simulated flow field visualization of the oscillatory angular motion of rectangular fin at different times steps. Images overlaid in MATLAB. The series of images demonstrate shedding of vortices in a similar manner.

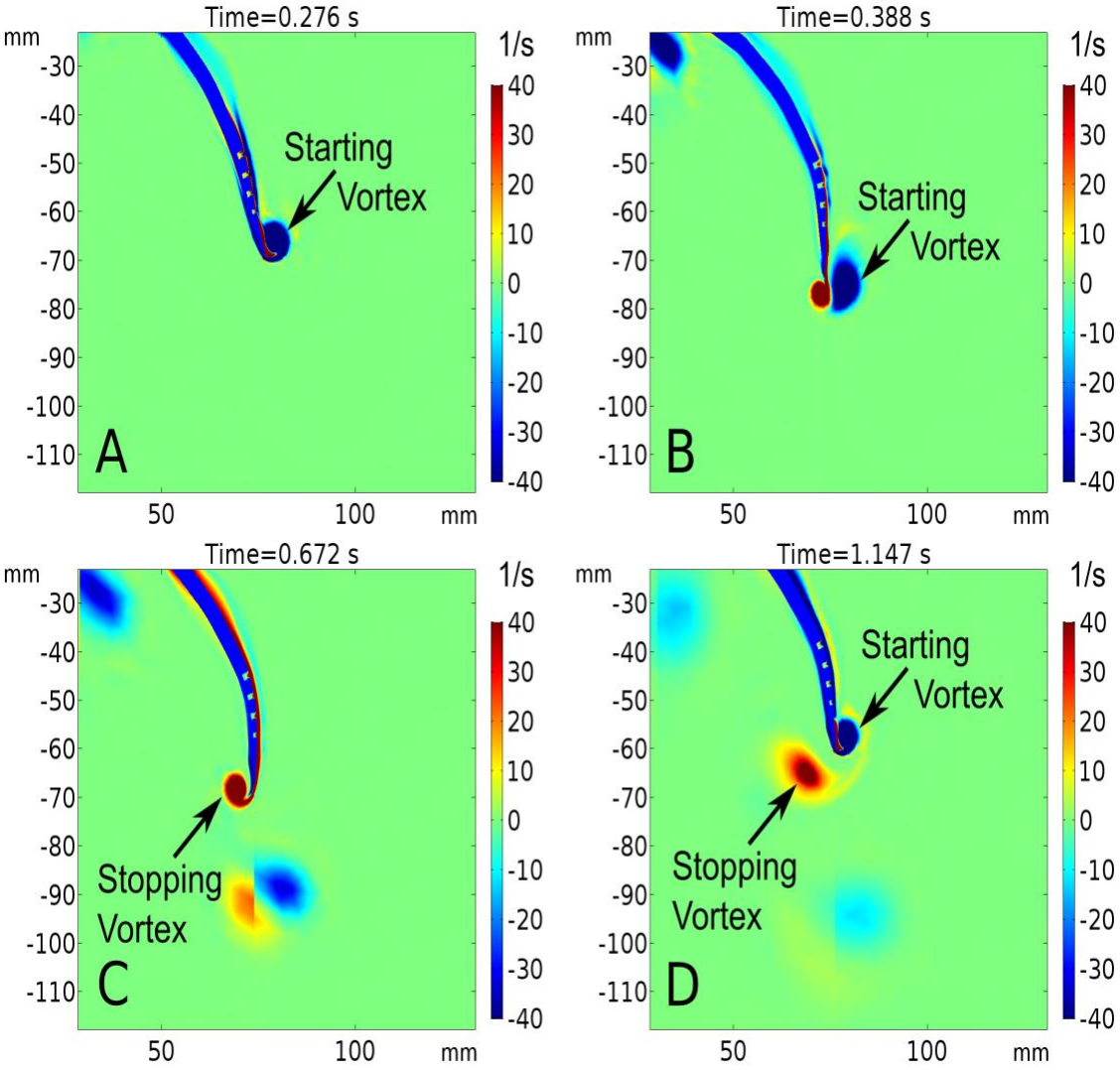

Figure 15. Fluid flow visualization at various stages of the cycle using vorticity plots generated by COMSOL Multiphysics. a) Starting vortex is forming near the margin of the bell at the start of contraction phase. b) Starting vortex shed and stopping vortex forming at the margin at the end of contraction phase. c) Stopping vortex shed near the end of relaxation phase. d) The starting vortex is forming again at the start of next contraction phase.

5. Conclusion

The numerical model simulates the flow pattern associated with the motion of jellyfish-based locomotor. The model demonstrates flow field similar to that seen in the experiment. We observe the formation and shedding of the starting and stopping vortices associated with the jellyfish propulsion as reported in the literature. The validation experiment with the rectangular fin demonstrates that the linear material model behaves similarly to the silicone rubbers. The linear model can thus be tuned to a specific structure and material to simulate a reasonably accurate motion. The complex jellyfish-based locomotor movement now can be easily manipulated. We can change the displacement functions to achieve the desired gaits. The displacement cycle comprises four stages, contraction, coasting, relaxation, and post relaxation period. We can change the amount of displacement, the time required for the complete cycle, and duration of each phase.

The numerical model thus allows flexibility in gait, amount of contraction, change in material properties, and change in geometry. The numerical model will also enable the researchers to study the effect of the change in the geometric and material structure of the locomotor on its motion. We can even simulate the impact of the change in the curvature. The simulation model eliminates the need for prototyping the locomotor for every change in the geometrical, structural, and material parameters. Using simulation, we save a lot of time and effort required to fabricate the locomotor.

In future, we aim to couple the thrust generated due to bell movement to the displacement of the locomotor. We would then be able to simulate the underwater travel of the locomotor completely. It will help in determining the efficiency of the locomotor.

We can run optimization studies on the model to get the set of optimal parameters for efficient propulsion.

Appendix A: MATLAB Code

1. Superimposing experiment and simulation images to estimate Young's modulus

```
% Cropping Images for the Modulus Experiment for Moldstar-30a
clear
clc
rect1 = [154.510000,50.510000,1035.980000,807.980000];
I1 = imread('Moldstar-30_100a.png');
I2 = imcrop(I1,rect1);
imshow(I2)
P1 = imread('DSC01053.JPG');
rect2 = [2630.510000,1820.510000,1176.980000,1518.980000];
P2 = imcrop(P1,rect2);
imshow(P2)
resizedI2=imresize(I2,[802 773]);
resizedP2=imresize(P2,[802 773]);
C = imfuse(resizedP2,resizedI2,'blend', 'Scaling', 'joint');
imshow(C)
```

2. Plotting simulated tip displacement data and exponential bounds to determine damping or viscoelastic parameters

```
%% Simulated Viscoelastic response of Moldstar-30 FC10
clear
clc
```

```
fileID = fopen('Moldstar-30_R-1(FC10).txt');
formatSpec = '%f %f';
feof(fileID)
C = textscan(fileID,formatSpec,'CommentStyle','%','Delimiter','\t');
hold on
C{1,1}(1:1350) = [];
C{1,2}(1:1350) = [];
C{1,1} = C{1,1}-1.35;
%scatter(C{1},C{2})
plot(C{1}, C{2}, 'b-')
fclose(fileID);
%% Bounding curve
t1 = 0:0.001:4;
T = 0.425;
zeta = 0.013809;
wn = 2*pi/T;
wd = wn*sqrt(1-zeta^2);
x = 11.5*exp(-t1*zeta*wd)/(sqrt(1-zeta^2));
plot(t1,x, 'r-')
mx = -11.5*exp(-t1*zeta*wd)/(sqrt(1-zeta^2));
plot(t1,mx,'r-')
hold off
%title('Simulated Rayleigh damping response of Mold Star 30 (Free length: 95 mm)')
```

```
xlabel('Time (sec)')

ylabel('Displacement (mm)')

legend('Simulated displacement','Exponential bounds')
```

3. Flapper control – Matlab code

```
%% flapper

clear, clc, close all

T = 1.25; %.75

StartAngle=96;

TwistAngle= 10; %10 %amplitude, not range

rtwbuild('Flapper_controller')

sim('Flapper_reader')

InPo.Time=InPo.Time./2

OuPo.Time=OuPo.Time./2

figure

hold on

plot(InPo,'b-')

plot(OuPo,'r-')

fplot(@(x) StartAngle+TwistAngle,[0,max(InPo.Time)],'k--')

fplot(@(x) StartAngle-TwistAngle,[0,max(InPo.Time)],'k--')

legend('input','output','goal','location','se')
```

4. Flapper control – Simulink file

Flapper controller

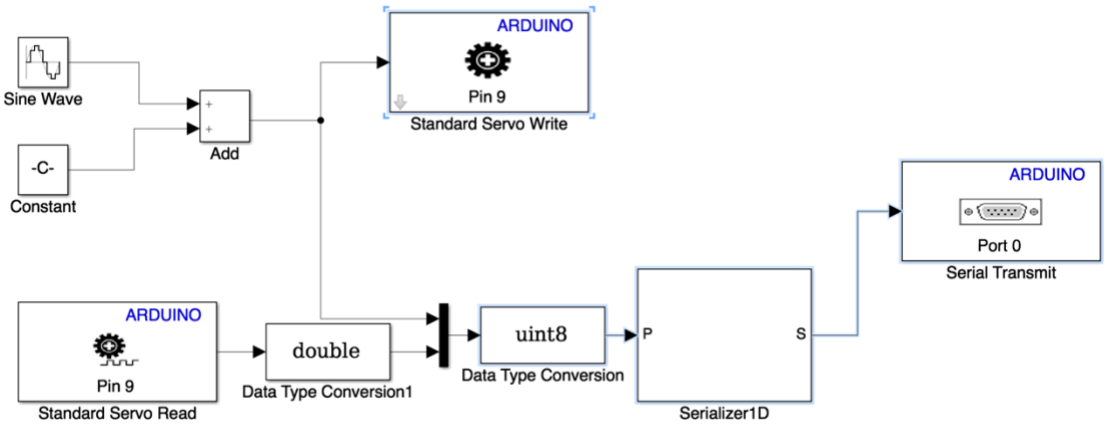

Flapper reader

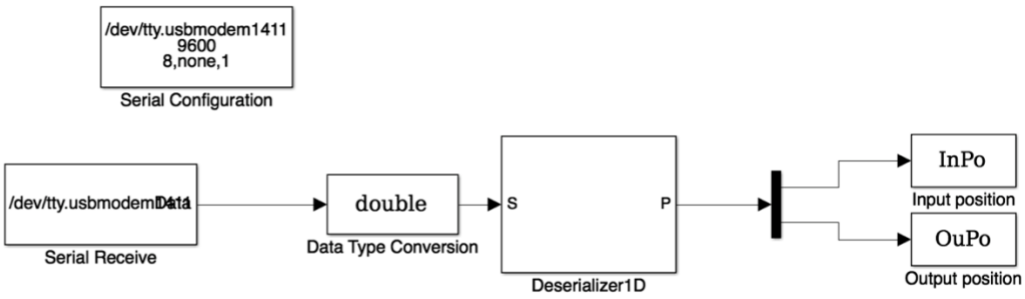

5. Comparing the simulated tip displacement for the validation experiment

```
% Comparison of Tip Displacement for Damping and Viscoelastic parameters
clear
clc
%% Rayleigh-1
fileID = fopen('Final(R:a-1,b-0.1).txt');
formatSpec = '%f %f';
feof(fileID)
```

```
R1 = textscan(fileID,formatSpec,'CommentStyle','%','Delimiter','\t');
hold on
plot(R1{1}, R1{2}, 'b-');
fclose(fileID);
%% Rayleigh-2
% fileID = fopen('Jelly--13a_Rayleigh2.txt');
% formatSpec = '%f %f';
% feof(fileID)
% R2 = textscan(fileID,formatSpec,'CommentStyle','%','Delimiter','\t');
% plot(R2{1}, R2{2}, 'r-');
% fclose(fileID);
%% Visco-1
fileID = fopen('Final_NoDamping.txt');
formatSpec = '%f %f';
feof(fileID)
V1 = textscan(fileID,formatSpec,'CommentStyle','%','Delimiter','\t');
plot(V1{1}, V1{2}, 'g-');
fclose(fileID);
%% Visco-2
% fileID = fopen('Jelly--13a_Visco2.txt');
% formatSpec = '%f %f';
% feof(fileID)
% V2 = textscan(fileID,formatSpec,'CommentStyle','%','Delimiter','\t');
```

```
% plot(V2{1}, V2{2}, 'r-');
% hold off
% fclose(fileID);
```

6. Comparing experiment and simulation tip displacement data for validation experiement

```
% Simulated Viscoelastic response of Moldstar-30 FC10
clear
clc

load('0tip_y.mat');
fileID = fopen('Jelly--13a_Rayleigh1.txt');
formatSpec = '%f %f';
feof(fileID)
C = textscan(fileID,formatSpec,'CommentStyle','%','Delimiter','\t');
C{1,1}(1:24) = [];
C{1,2}(1:24) = [];
C{1,1} = C{1,1}-0.115;
%scatter(C{1},C{2})
hold on
plot(C{1}, C{2}, 'b-','LineWidth',2);
%%
t =t/60;
```

```
y_smooth=smooth(t,y_corrected, 0.05, 'rloess');
plot(t,y_smooth,'r-','LineWidth',2);
hold on
%plot(t,y_corrected);
fclose(fileID);
grid on
xlabel('Time (s)','FontSize',20)
ylabel('Displacement (mm)', 'FontSize', 20)
legend('Simulation','Experimental')
xlim([0 10])
set(gca,'FontSize',16)
```

7. Splicing video into individual frames

```
% Video to Image Sequences
clear
clc
vid = VideoReader('0Jelly--13a_R2(Vorticity).mov');
 i =1;
while hasFrame(vid)
    frames = readFrame(vid);
    filename = [sprintf('sim_Image_0%04d', i) '.jpg'];
    imwrite(frames,filename); % ['Image' int2str(i), '.jpg']
    %bwframe = rgb2gray(imread(filename)); % ['Image' int2str(i), '.jpg']
```

```
    %imwrite(bwframe,filename); % ['Image' int2str(i), '.jpg']
%     if i==1
%         break
%     end
    i = i+1;
 end
```

8. Creating video from individual frames

```
%Write Video from Picture Files
vid=VideoWriter('0Fin_exp_sim.mp4');
vid.FrameRate=25;
open(vid);
for i=1:599
    pic=[sprintf('bl_exp-sim_Image_0%04d', i) '.jpg'];
    frame=imread(pic);
    writeVideo(vid,frame);
end
close(vid);
```

9. Superimposing PIV and simulation images

```
% Cropping Images for the Modulus Experiment for Ecoflex-30
% Author: Ajay Dusane
clear
```

```
clc
for i=1:599
    gefilename = [sprintf('r_Image_0%04d', i) '.jpg']; %piv_Image_%03d
    I1 = imread(gefilename);%imread('geImage_00001.jpg');
    I3=imresize(I1,[963 1861]);
    rect1 = [2.51000,0.51000,1374,899]; %[2.51000,0.51000,1374,899] for rImage
    I2 = imcrop(I3,rect1);
%B=imrotate(I2,-4);
%imshow(I2)
gsfilename = [sprintf('sim_Image_0%04d', i) '.jpg'];
    P1 = imread(gsfilename);%imread('fs_d_Image_00001.jpg');
    rect2 = [616.51000,285.51000,879.9800,548.98000];
    P2 = imcrop(P1,rect2);
%imshow(P2)
resizedI2=imresize(I2,[802 1000]);
    resizedP2=imresize(P2,[802 1000]);
C = imfuse(resizedP2,resizedI2,'blend', 'Scaling', 'joint');
    blfilename = [sprintf('bl_exp-sim_Image_0%04d', i) '.jpg'];
    imwrite(C,blfilename);
end
imshow(C)
```

References

[1] S. P. Colin and J. H. Costello, "Morphology, swimming performance and propulsive mode of six co-occurring hydromedusae," *J. Exp. Biol.*, vol. 205, no. 3, pp. 427–437, Feb. 2002.

[2] J. O. Dabiri, S. P. Colin, J. H. Costello, and M. Gharib, "Flow patterns generated by oblate medusan jellyfish: field measurements and laboratory analyses," *J. Exp. Biol.*, vol. 208, no. 7, pp. 1257–1265, Apr. 2005.

[3] J. H. Costello and S. P. Colin, "Morphology, fluid motion and predation by the scyphomedusa Aurelia aurita," *Mar. Biol.*, vol. 121, no. 2, pp. 327–334, Dec. 1994.

[4] B. J. Gemmell *et al.*, "Passive energy recapture in jellyfish contributes to propulsive advantage over other metazoans," *Proc. Natl. Acad. Sci.*, vol. 110, no. 44, pp. 17904–17909, Oct. 2013.

[5] T. L. Daniel, "Mechanics and energetics of medusan jet propulsion," *Can. J. Zool.*, vol. 61, no. 6, pp. 1406–1420, Jun. 1983.

[6] T. L. Daniel, "Cost of Locomotion: Unsteady Medusan Swimming," *J. Exp. Biol.*, vol. 119, no. 1, pp. 149–164, Nov. 1985.

[7] L. Kozlowski, "Jellyfish a model of efficiency," *Los Angeles Times*, 06-Nov-2010.

[8] J. O. Dabiri and M. Gharib, "Sensitivity analysis of kinematic approximations in dynamic medusan swimming models," *J. Exp. Biol.*, vol. 206, no. 20, pp. 3675–3680, Oct. 2003.

[9] J. O. Dabiri and M. Gharib, "Fluid entrainment by isolated vortex rings," *J. Fluid Mech.*, vol. 511, pp. 311–331, 2004.

[10] J. O. Dabiri and M. Gharib, “The role of optimal vortex formation in biological fluid transport,” *Proc. R. Soc. B Biol. Sci.*, vol. 272, no. 1572, pp. 1557–1560, Aug. 2005.

[11] J. O. Dabiri, S. P. Colin, and J. H. Costello, “Fast-swimming hydromedusae exploit velar kinematics to form an optimal vortex wake,” *J. Exp. Biol.*, vol. 209, no. 11, pp. 2025–2033, Jun. 2006.

[12] J. O. Dabiri, “Optimal Vortex Formation as a Unifying Principle in Biological Propulsion,” *Annu. Rev. Fluid Mech.*, vol. 41, no. 1, pp. 17–33, 2009.

[13] J. O. Dabiri, S. P. Colin, K. Katija, and J. H. Costello, “A wake-based correlate of swimming performance and foraging behavior in seven co-occurring jellyfish species,” *J. Exp. Biol.*, vol. 213, no. 8, pp. 1217–1225, Apr. 2010.

[14] K. B. Joshi, J. H. Costello, and S. Priya, “Estimation of Solar Energy Harvested for Autonomous Jellyfish Vehicles (AJVs),” *IEEE J. Ocean. Eng.*, vol. 36, no. 4, pp. 539–551, 2011.

[15] J. C. Nawroth *et al.*, “A tissue-engineered jellyfish with biomimetic propulsion,” *Nat. Biotechnol.*, vol. 30, no. 8, pp. 792–797, Aug. 2012.

[16] “3D simulations of self-propelled, video reconstructed jellyfish using vortex methods - DTU Orbit.” [Online]. Available: http://orbit.dtu.dk/en/activities/3d-simulations-of-selfpropelled-video-reconstructed-jellyfish-using-vortex-methods(ff90c083-9c17-45af-9d3a-576823378eb0).html. [Accessed: 17-Nov-2017].

[17] A. Villanueva, C. Smith, and S. Priya, “A biomimetic robotic jellyfish (Robojelly) actuated by shape memory alloy composite actuators,” *Bioinspir. Biomim.*, vol. 6, no. 3, p. 036004, Sep. 2011.

[18] J. S. Najem, “Design and Development of a Bio-inspired Robotic Jellysh that Features Ionic Polymer Metal Composites Actuators,” thesis, Virginia Tech, 2012.

[19] K. Yang, M. Cotton, J. Xie, Y. Wang, and A. D. Mazzeo, “An Agile, Hydraulic Jellyfish-based Soft Robot,” *Prep.*, 2016.

[20] B. W. Oudheusden, F. Scarano, E. W. M. Roosenboom, E. W. F. Casimiri, and L. J. Souverein, “Evaluation of integral forces and pressure fields from planar velocimetry data for incompressible and compressible flows,” *Exp. Fluids*, vol. 43, no. 2–3, pp. 153–162, Feb. 2007.

[21] T. Baur and J. Köngeter, “PIV with high temporal resolution for the determination of local pressure reductions from coherent turbulence phenomena,” *3rd Int. Workshop Part. Image Velocim.*, 1999.

[22] W. Thielicke and E. J. Stamhuis, “PIVlab – Towards User-friendly, Affordable and Accurate Digital Particle Image Velocimetry in MATLAB,” *J. Open Res. Softw.*, vol. 2, Oct. 2014.

[23] W. Thielicke and E. J. Stamhuis, “PIVlab - Time-Resolved Digital Particle Image Velocimetry Tool for MATLAB.” 25-Mar-2015.

[24] W. Thielicke, “The flapping flight of birds: Analysis and application,” [S.n.], 2014.

[25] K. Yang, “A Hydraulic Jellyfish-based Soft Robot with Passive Energy Recapture,” Masters Thesis, Rutgers University, Piscataway, NJ, 2015.

[26] N. Cheney, R. MacCurdy, J. Clune, and H. Lipson, “Unshackling Evolution: Evolving Soft Robots with Multiple Materials and a Powerful Generative Encoding,”

in *Proceedings of the 15th Annual Conference on Genetic and Evolutionary Computation*, New York, NY, USA, 2013, pp. 167–174.

[27] B. J. Gemmell, J. H. Costello, J. O. Dabiri, and S. P. Colin, "Suction-based propulsion as a basis for efficient animal swimming," *Nat. Commun.*, vol. 6, p. 8790, Nov. 2015.

[28] P. Valdivia y Alvarado and K. Youcef-Toumi, "Design of Machines With Compliant Bodies for Biomimetic Locomotion in Liquid Environments," *J. Dyn. Syst. Meas. Control*, vol. 128, no. 1, pp. 3–13, Sep. 2005.

[29] C. Prince, W. Lin, J. Lin, S. D. Peterson, and M. Porfiri, "Temporally-resolved hydrodynamics in the vicinity of a vibrating ionic polymer metal composite," *J. Appl. Phys.*, vol. 107, no. 9, p. 094908, May 2010.

[30] M. Aureli and M. Porfiri, "Low frequency and large amplitude oscillations of cantilevers in viscous fluids," *Appl. Phys. Lett.*, vol. 96, no. 16, p. 164102, Apr. 2010.

[31] M. S. Triantafyllou, G. S. Triantafyllou, and R. Gopalkrishnan, "Wake mechanics for thrust generation in oscillating foils," *Phys. Fluids Fluid Dyn.*, vol. 3, no. 12, pp. 2835–2837, Dec. 1991.

[32] J. E. Sader, "Frequency response of cantilever beams immersed in viscous fluids with applications to the atomic force microscope," *J. Appl. Phys.*, vol. 84, no. 1, pp. 64–76, Jun. 1998.

[33] S. Mondal and S. Chakraborty, *An Inverse Approach for the Determination of Viscous Damping Model of Fibre Reinforced Plastic Beams using Finite Element Model Updating*, vol. 21. 2016.

[34] A. P. Maertens, A. Gao, and M. S. Triantafyllou, “Optimal undulatory swimming for a single fish-like body and for a pair of interacting swimmers,” *J. Fluid Mech.*, vol. 813, pp. 301–345, Feb. 2017.

[35] M. Sahin, K. Mohseni, and S. P. Colin, “The numerical comparison of flow patterns and propulsive performances for the hydromedusae Sarsia tubulosa and Aequorea victoria,” *J. Exp. Biol.*, vol. 212, no. 16, pp. 2656–2667, Aug. 2009.

[36] M. Sfakiotakis, D. M. Lane, and J. B. C. Davies, “Review of fish swimming modes for aquatic locomotion,” *IEEE J. Ocean. Eng.*, vol. 24, no. 2, pp. 237–252, Apr. 1999.

[37] R. E. D. Bishop and A. Y. Hassan, “The Lift and Drag Forces on a Circular Cylinder Oscillating in a Flowing Fluid,” *Proc. R. Soc. Lond. Ser. Math. Phys. Sci.*, vol. 277, no. 1368, pp. 51–75, 1964.

[38] Z. Chen, S. Shatara, and X. Tan, “Modeling of Biomimetic Robotic Fish Propelled by An Ionic Polymer #x2013;Metal Composite Caudal Fin,” *IEEEASME Trans. Mechatron.*, vol. 15, no. 3, pp. 448–459, Jun. 2010.

[39] M. Aureli, V. Kopman, and M. Porfiri, “Free-Locomotion of Underwater Vehicles Actuated by Ionic Polymer Metal Composites,” *IEEEASME Trans. Mechatron.*, vol. 15, no. 4, pp. 603–614, Aug. 2010.

[40] F. G. Serchi, A. Arienti, and C. Laschi, “Biomimetic Vortex Propulsion: Toward the New Paradigm of Soft Unmanned Underwater Vehicles,” *IEEEASME Trans. Mechatron.*, vol. 18, no. 2, pp. 484–493, Apr. 2013.

[41] L. Dai, G. He, and X. Zhang, “Self-propelled swimming of a flexible plunging foil near a solid wall,” *Bioinspir. Biomim.*, vol. 11, no. 4, p. 046005, 2016.